Transient interactions studied by NMR : iron sulfur proteins and their interaction partners

Xu, X.

The Ternary Protein Complex of Ferredoxin, Ferredoxin/thioredoxin Reductase, and Thioredoxin Studied by NMR

Abstract:

In oxygenic photosynthetic cells, carbon metabolism is regulated by a light-dependent redox signaling pathway through which the light signal is transmitted in the form of electrons via a redox chain comprising ferredoxin (Fd) , ferredoxin:thioredoxin reductase (FTR), and thioredoxin (Trx). Trx affects the activity of a variety of enzymes via dithiol oxidation and reduction reactions. FTR reduces an internal disulfide bridge of Trx and Trx reduction involves a transient crosslink with FTR. In this study, NMR spectroscopy was used to investigate the interaction of Fd, FTR, and *m*-type Trx. NMR titration experiments indicate that FTR uses distinct sites to bind Fd and Trx simultaneously to form a non-covalent ternary complex. The orientation of Trx-*m* relative to FTR was determined from the intermolecular paramagnetic broadening caused by the 4Fe-4S cluster of FTR. A model of the non-covalent binary complex of FTR/Trx-*m* was obtained through restraint-filtered soft docking, using the paramagnetic distance restraints. The model suggests that a rotational movement of Trx takes place when the non-covalent binary complex proceeds to the covalent complex. This study shows that paramagnetic NMR and X-ray diffraction of crystals are complementary in the elucidation of dynamics in a transient protein complex.

Introduction

Photosynthesis produces nearly all of the organic carbon in the biosphere. In this process, light not only provides the energy and reducing power (ATP and NADPH) required to drive the Calvin cycle, but also serves as a regulatory factor for the activity of enzymes involved in carbon assimilation. In oxygenic photosynthetic cells, carbon metabolism is regulated by a light-dependent redox signaling pathway in which ferredoxin:thioredoxin reductase (FTR) plays a central role [(1)]. The light signal is transmitted in the form of electrons from the chlorophyll-containing thylakoid membrane via a plant type ferredoxin (Fd), FTR, and chloroplastic *m*-type or *f*-type thioredoxins (Trx-*m* and Trx-*f*), which can activate or deactivate a variety of target enzymes by dithiol-disulfide interchange. Many biochemical and structural investigations have been carried out on the components of this redox cascade [(1,2,3)].

FTR is a disk-shape molecule with a width of about 10 Å across the center. It is an αβ-heterodimer composed of a 12 kDa catalytic subunit in which a 4Fe-4S cluster is located and a variable subunit with a size ranging from 7 to 13 kDa between different species [(4)]. The catalytic domain of FTR has seven highly conserved cysteine residues, six of which are organized in two Cys-cisPro-Cys (CPC) and one Cys-His-Cys (CHC) motifs. In the FTR from *Synechocystis* sp PCC 6803, C57 and C87 form the active site disulfide, and other four cysteines, C55, C74, C76 and C85, are ligands of the 4Fe-4S cluster. X-ray diffraction studies on crystals suggest that Fd and Trx-*m* dock on opposite sides of FTR, enabling the simultaneous interaction of FTR with the electron donor and acceptor [(5)].

A two-step reaction mechanism of the reduction of Trx by FTR has been proposed based on spectroscopic measurements [(6,7,8)] and was supported by recent X-ray diffraction studies [(5)]. The mechanism involves the unique 4Fe-4S

cluster and a disulfide bridge within FTR. In the resting enzymes, a weak interaction between the iron cluster and the disulfide cysteines was suggested from Mössbauer spectroscopic study [8]. When the first electron is transferred from Fd to FTR, a one-electron-reduced intermediate is formed. The active site disulfide of FTR is cleaved and the exposed Cys57 forms a transient intermolecular disulfide bond with a cysteine on Trx. The other Cys of the FTR disulfide bond, Cys87 meanwhile coordinates with 4Fe-4S cluster. It was confirmed with *N*-ethylmaleimide (NEM) modified FTR that the one-electron-reduced FTR indeed is a reaction intermediate [6,5]. The second electron, transferred by another molecule of Fd, reduces the cluster-ligated cysteine 87 and re-establishes the original 4Fe-4S^{2+} cluster. The newly released cysteine 87 attacks and cleaves the hetero-disulfide bond between FTR and Trx, enabling the formation of reduced Trx. Thus, the role of the 4Fe-4S cluster involves more than the mere catalysis of electron transfer from Fd to Trx. The five-coordinated cluster stabilizes the one-electron-reduced intermediate, enabling the reaction between two one-electron carriers (Fd) to one two-electron carrier (Trx), without the release of reactive intermediates. In the recent X-ray diffraction study, crystal structures of trapped intermediate states including the cross-linked binary complexes of FTR with Trx mutants and the ternary complex of Fd with cross-linked FTR/Trx were obtained, providing convincing evidence for the proposed reaction mechanism.

In this study, two-dimensional NMR spectroscopy was used to study the interaction of Fd, FTR, and Trx-*m*. NMR titration experiments indicate that FTR can bind to Fd and Trx-*m* simultaneously to form a non-covalent ternary complex in solution. Utilizing the paramagnetism caused by the 4Fe-4S^{2+} cluster of FTR, the binding site for FTR on Trx-*m* in the non-covalent complex was determined. The interaction interface of Trx-*m* includes the active site in the Trx WCXXC motif and neighboring residues. A docking model of the non-covalent binary complex of FTR/Trx-*m* was obtained through restrained-filtered docking,

using paramagnetic distance restraints. The comparison of the solution model of non-covalent FTR/Trx-*m* binary complex with the crystal structure of cross-linked complex suggests that a rotational movement is required for the non-covalent complex to proceed to the cross-linked intermediate.

Materials and methods

Protein production and purification

The production and purification of Fd and FTR has been reported [9]. For the production of ^{15}N labeled thioredoxin a culture of *Escherichia coli* BL21 (DE3) harboring a plasmid derived from pET28b and encoding spinach Trx-*m* with a N-terminal His tag was incubated in minimal medium containing $^{15}NH_4Cl$ (0.5 g/L) and kanamycin (50 mg/L) at 37 ºC until the OD_{600} was 0.6. Then IPTG (Isopropyl-β-D-thiogalactopyranoside) was added to a final concentration of 1 mM, and incubation was continued for 16 hrs in M9 medium at 30 ºC. Cells were harvested by centrifugation, resuspended in 50 mM sodium phosphate buffer (pH 8.0) containing 200 mM NaCl, passed five times through a French Press at 18000 psi, and centrifuged at 50,000 rpm for 1 hr. The supernatant was filtered through 0.45 μm pore-size membrane and applied to a Ni^{2+} affinity column (HisTrap Chelating HP, obtained from Amersham Bioscience) incorporated into a BioCAD perfusion chromatography system (PerSeptive BioSciences). The column was washed with 50 mM sodium phosphate buffer (pH 8.0) containing 500 mM NaCl (buffer A), supplemented with 10 mM imidazole, followed by a wash with buffer A containing 125 mM imidazole. The His-tagged proteins were then eluted with buffer containing 250 mM imidazole. The elution buffer was exchanged for 50 mM sodium phosphate buffer by ultrafiltration using the Amicon YM10 membrane. The concentration of Trx-*m* was determined from the predicted absorbance at 280 nm ($\varepsilon = 22.2\ mM^{-1}cm^{-1}$).

NMR measurements

All NMR samples contained 20 mM sodium phosphate buffer, pH 6.5, and 5% D_2O. All NMR experiments were conducted on a Bruker DMX 600 spectrometer equipped with TCI-Z-GRAD cryoprobe. For ^{15}N labeled oxidized Trx-*m*, the backbone amide assignments were obtained using a ^{1}H-^{15}N HSQC spectrum and three-dimensional ^{1}H-^{15}N TOCSY-HSQC and ^{1}H-^{15}N NOESY-HSQC spectra measured at 298 K. NMR data-processing was performed using AZARA (http://www.bio.cam.ac.uk/pub/azara) and the spectra were analyzed in Ansig-for-Windows[10].

On the basis the available proton assignments of spinach Trx-*m* [11], most of ^{1}H and ^{15}N resonances of backbone NH groups were assigned, except for some overlapping cross-peaks. Residues without backbone amide assignment are E4, A5, E8, V9, S24, W36, G38, and I77. The indole side chain NH groups of W33 and W36 were assigned based on previous proton assignments.

In titration experiments, ^{1}H-^{15}N HSQC spectra were recorded on samples of 0.2 mM ^{15}N Trx-*m* into which unlabeled FTR stock was titrated. To observe the ternary complex formation, a HSQC spectrum was first recorded on a sample of 0.2 mM ^{15}N Trx-*m*, then 2 mM unlabeled FTR was titrated into ^{15}N Trx-*m* to a molar ratio of 1:1. Finally, microliter aliquots of highly concentrated ^{15}N labeled Fd were added to the binary FTR/Trx-*m* complex to a molar ratio of 3.2 (Fd over FTR).

Docking and modeling

Trx-*m* residues were categorized into three groups based on the paramagnetic relaxation enhancement effect that they experienced. Resonances that disappeared early in the titration experienced large paramagnetic effects (class I), those that disappeared later weak ones (class II). The remaining residues formed class III. The paramagnetic effects were translated to loose distance restraints. For calibration of these distances, effects observed in an earlier study on two

residues, Cys 39 and Ala40 of Ga substituted Fd bound to FTR were used[9]. The resonances of these residues disappeared during a similar NMR titration and are known to be 15 to 18 Å away from the 4Fe-4S cluster in the Fd:FTR complex [5]. For class I, the distance between the geometrical center of the 4Fe-4S cluster and amide nitrogen were restrained with a lower bound 10 Å and upper bound 15 Å. For class II, a lower bound of 10 Å and an upper bound of 20 Å were applied. For residues in class III, a lower bound of 18 Å and an upper bound of 38 Å were used.

Docking calculations were carried out with the program BIGGER (Bimolecular complex generation with Global Evaluation and Ranking) [12]. Structure coordinates of free FTR (PDB access code: 1DJ7) and Trx-*m* (1FB7) [13] were used as inputs for the docking. FTR is the target and Trx-*m* is the probe for searching for the possible solutions of the complex geometry. For each orientation of two proteins, optimal surface matching was first achieved by translational shifting the probe matrix relative to the target matrix. The probe was also rotated by 15° for each step until a complete search was performed. All solutions containing unrealistic steric clashes were discarded, but the side chains of residues Arg, Lys, Asp, Glu, and Met were allowed to penetrate up to the core of the other proteins as long as there is no unrealistic interpenetration. The ensemble of the top 5000 model structures was used for the subsequent cluster analysis. The experimental distance restraints derived from intermolecular paramagnetic relaxation enhancement were used to filter out the structures that were in agreement with the NMR data.

Results

The binary complex of FTR and Trx

A titration experiment was performed by recording ^{15}N-^{1}H HSQC spectra of Trx-*m* upon addition of small aliquots of unlabeled FTR. Changes in NMR

signal intensities and chemical shift changes were monitored in order to determine the characteristics of the interaction. During the first four titration points, to a Trx:FTR ratio of 1: 0.27, some residues show fast intensity decrease and significant line broadening. At the 7th titration point, with a ratio 1: 0.54, many peaks had disappeared whereas some resonances show small chemical shift changes. In the final titration point, the chemical shift changes of those residues were saturated, suggesting that all the Trx-*m* was in a bound state in the presence of an excess of FTR. The k_{off} is estimated to be > 100 s^{-1} and K_a of the binding is at least 10^6 M^{-1}. For those residues that disappeared during the tirtration, no cross-peaks reappeared for the last titration point representing the fully bound state of Trx/FTR (Figure 6.1). This phenomenon can be attributed to the combined broadening due to the complex formation and intermolecular paramagnetic relaxation enhancement (PRE) that originates from the iron sulfur cluster of FTR. The broadening effects can not be due to exchange broadening only, because resonances of the bound form would be expected to become visible at the end of the titration.

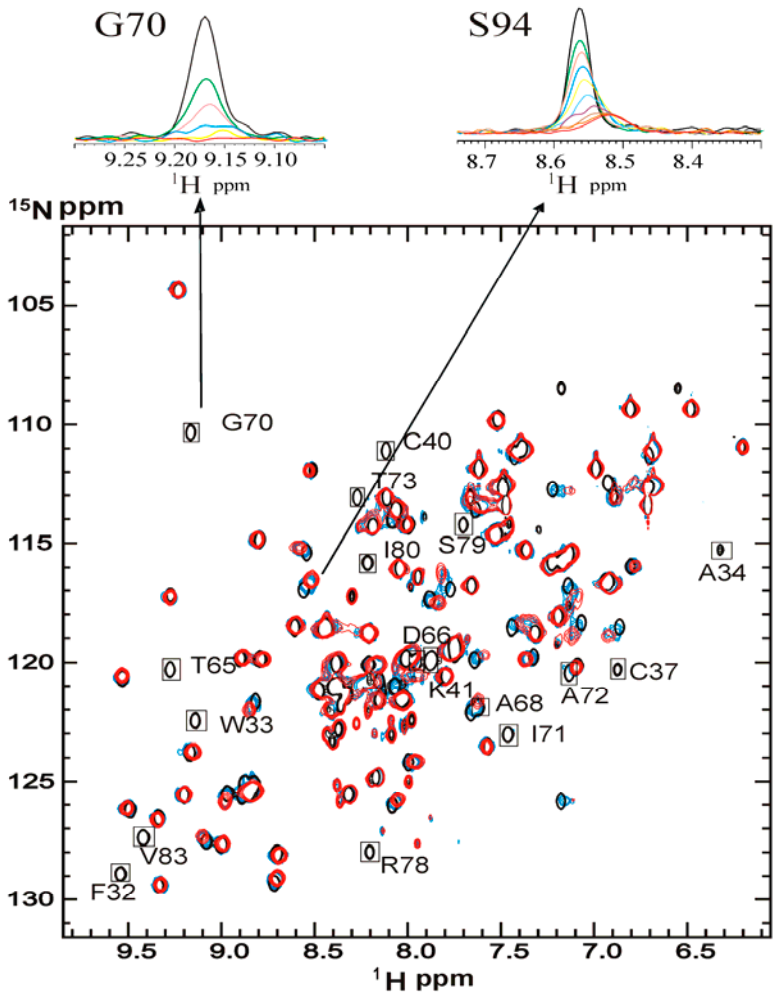

Figure 6.1. Overlay of ^{1}H-^{15}N HSQC spectra of ^{15}N Trx-*m* in the titration experiments. Black: Free Trx-*m*; Cyan: Trx-*m*/FTR at a ratio of 1:0.54; Red: ratio 1:1.26. The resonances of the residues experiencing a PRE effect in FTR/Trx-*m* complex are labeled. The cross-section along the F2 dimension through the $^1H^N$ resonances of residues G70 and S94 at different titration points are shown in the top panel. The slices show the ratios of FTR/Trx-*m* of 0, 0.09, 0.18, 0.27, 0.36, 0.54, 0.72, 0.99, 1.17, 1.26 in black, green, pink, blue, yellow, cyan, purple, brown, orange and red, respectively.

Interaction mapping based on detection of intermolecular PRE

Residues of Trx-*m* experiencing intermolecular PRE upon complex formation with FTR were mapped onto the protein surface of Trx-*m* to visualize the binding map (Figure 6.2). The residues experiencing the paramagnetic effect can

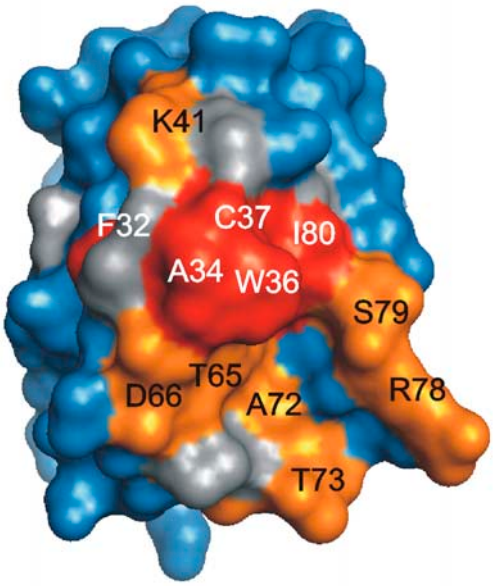

Figure 6.2. Surface representation of Trx-m showing the interaction area (PDB access code: 1FB6) in the non-covalent FTR/Trx-*m* complex. Residues experiencing strong and weak paramagnetic effects of 4Fe-4S are in red and orange, respectively. Residues that experience no paramagnetic effect are in blue. Residues without assignment are in gray.

be classified into two groups. One group comprising the residues F32, A34, C37 and I80 show a fast intensity drop during the first four titration points, suggesting that their backbone amides get close to the cluster and experience strong paramagnetism in the complex. The cross-peak of indole side chain NH^{ε} group of W36 has completely disappeared after the third titration point. W36 is also in the core of interface. Other residues, experiencing less PRE, are located

around the core interface, including the charged residues K41, D66, R78, polar residues T65, T73, and S79, and the non-polar residues A68, G70, I71, A72, and V83. The interaction interface of Trx-*m* in the complex FTR/Trx-*m* includes the typical WCXXC motif and peripheral residues.

The orientation of Trx-m in the complex with FTR

PRE results from the magnetic dipolar interaction between a nucleus and the unpaired electrons in a metal center or stable radical. The magnitude of PRE is proportional to the reciprocal sixth power of the distance between the nucleus and the metal center. Because of the large magnetic moment of an unpaired electron, effects can be observed over large distances. The intrinsic metal sites from some metallo-proteins can serve as good paramagnetic probes for the study of bimolecular interactions. Therefore, the paramagnetic broadening of Trx-*m* residues was converted into distance restraints to assist docking calculations of Trx-*m* onto FTR.

The 4Fe-4S cluster of FTR is constituted of two Fe^{3+} and Fe^{2+}. The ground state is S = 0, but magnetically active states are populated at room temperature. Previously, a gallium-Fd, a diamagnetic structural analog of Fd, was used to determine the complete interaction site of Fd in the FTR/Fd complex in solution. Two residues (C39 and A40) of Fd were suggested to sense the intermolecular PRE effect in the FTR/Fd complex [(9)]. The distances of amide C39 and A40 of Fd to the 4Fe-4S cluster of FTR in the crystal structural of the Fd/FTR complex were used to calibrate of the strength of the paramagnetism of 4Fe-4S iron sulfur cluster. The Trx-*m* residues were categorized into three classes associated with loose distance restraints, on the basis of the observed PRE effects. Lower and upper bounds of 10 and 15 Å of the distance between the amide nitrogen and the 4Fe-4S cluster center were applied to the residues with strong PRE effects (class I). Lower and upper bounds of 10 and 20 Å were used for residues with small

PRE (class II). The bounds were set to of 18 and 38 Å (class III) for the residues without intermolecular PRE effects.

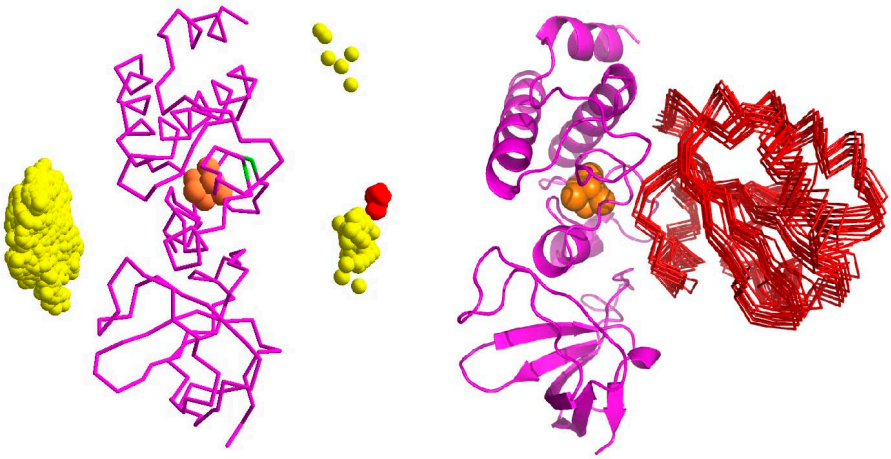

Figure 6.3. The docking solutions of the FTR/Trx-*m* complex. Left: FTR is indicated by purple C^{α} trace and the 4Fe-4S cluster is shown as orange spheres and C57 and C87 are in green. The geometrical centers of Trx-*m* of 5000 solutions are represented by yellow spheres. The top ten solutions based on PRE restraints scoring are in red. Right: The ensemble of top ten structures with FTR superimposed. Trx-*m* structure are shown as C^{α} trace and FTR as ribbons.

A docking calculation was performed using the BIGGER software to obtain the possible conformations of the non-covalent binary complex of FTR/Trx-*m*. The program selected an initial set of orientations of Trx-*m* during a systematic search of the conformational space, scored on the basis of geometric complementarities and electrostatic interactions. All solutions were then scored and clustered using the distance restraints derived from the PRE data (see materials and methods). The geometrical centers of Trx-*m* are shown for these orientations as yellow spheres in Figure 6.3. Interestingly, two clusters are found on opposite sides of FTR. The cluster on the left in Fig 3 is in fact the side where Fd binds. This side cannot be the Trx binding site because it places Trx far from

the FTR active site Cys57 which forms the transient inter-disulfide bridge with Trx. The best ten solutions are shown as the small red cluster on the right of FTR in Fig 3. In these conformations, the active site residues of Trx-*m* are close to the intra-disulfide of FTR and the short helix formed by G70-T73 is docked into the concave region formed by the catalytic subunit and variable unit of FTR.

Ternary complex formation

A titration experiment using ^{15}N labeled Trx-*m*, ^{15}N labled Fd and unlabled FTR was carried out to investigate the non-covalent ternary complex formation. When FTR was titrated into the ^{15}N labeled Trx-*m* to a molar ratio of 1.0, the complex formation between FTR and Trx-*m* was indicated by the line broadening or small chemical shift changes of resonances of Trx-*m* as described above. Then, ^{15}N labeled Fd was further titrated into the binary complex. Although the introduction of the second ^{15}N labeled sample results in a crowded HSQC spectrum, a well-dispersed region of HSQC can be used to monitor the association or dissociation of different components. The intensity change and chemical shift change pattern of residue 93 of Fd are the same as those observed in the binary complex of FTR and Fd [(9)], which indicates the association of Fd with FTR. No further chemical shift changes of residues of Trx-*m* are observed when Fd is titrated into the binary complex, suggesting the Trx-*m* remains bound and unperturbed when Fd associates the FTR (Figure 6.4 c, d, e). It is concluded that a non-covalent ternary complex Fd:FTR:Trx-*m* is formed in solution.

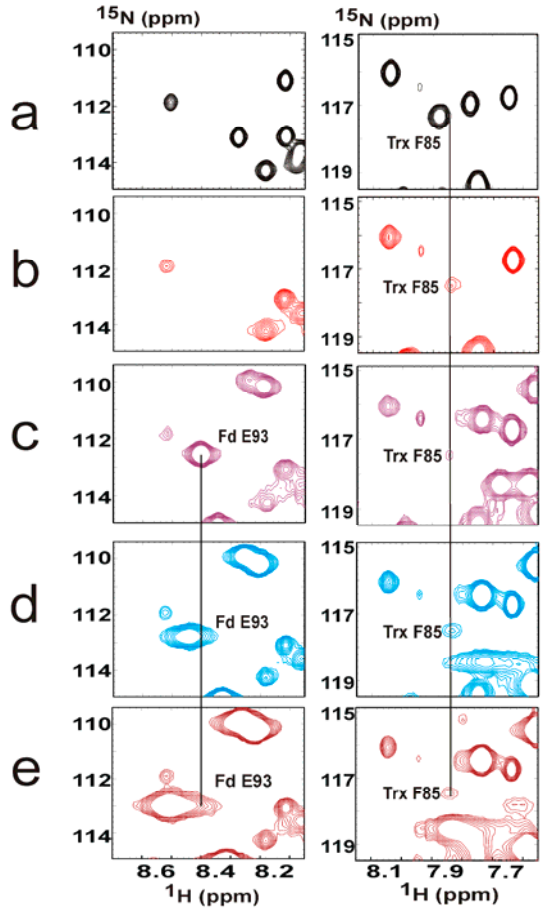

Figure 6.4. Formation of non-covalent ternary complex of Fd, FTR and Trx-*m*, evidenced from HSQC titration experiment. The association of FTR with Trx-*m* was evidenced by a chemical shift change and linebroadening of the resonance of Trx-*m* F85. The association of Fd with FTR was monitored by observing the behavior of the resonance of Fd E93. a: ^{15}N-^{1}H HSQC of free ^{15}N Trx-*m* b: ^{15}N Trx :FTR (1:1); c: ^{15}N Trx :FTR: ^{15}Fd (1:1:1); d: ^{15}N Trx :FTR: ^{15}NFd (1:1:2); e: ^{15}N Trx :FTR: ^{15}NFd (1:1:3.2). The vertical lines indicate the resonance positions for the bound state of Fd E93 (left) and Trx-*m* F85 (right), respectively.

Discussion

Comparison of the interaction interface of Trx-m in different complexes

A comparison of the interface of Trx-*m* in the non-covalent complex with that in the cross-linked complex suggests some identical interactions and some different ones. Both interfaces include the WCXXC motif and several residues around the active disulfide bridge of Trx-*m*. In the crystal structure of cross-linked FTR/Trx-*m* complex, only one charged residue (R78) is present in the interfaces, but not involved any salt bridge formation with residues of FTR, whereas in the non-covalent complex the interface contain R78 and D66. The fact that more charged residues are involved in the initial non-covalent interaction of FTR/Trx-*m* but no salt bridges are formed in the crosslinked complex may suggests that these charged residues only function as general attractants for the fast association [(14)].

Comparison of non-covalent complex with the cross-linked binary complex of FTR/Trx-m

For both the model of the non-covalent complex and the crystal structure of the crosslinked reaction intermediate FTR/Trx-*m*C40S, the distance between the amide nitrogen and FTR 4Fe-4S cluster was measured for each residue. In Figure 6.5 these distances are compared with the NMR derived distance restraints. The upper and lower bounds are indicated by the blue and red lines, respectively. For residues affected by PRE, 10 Å was used as lower bound to avoid the steric clashes. Two different upper bounds, 15 and 20 Å were used for strongly and weakly affected residues, respectively. For residues without PRE effect, 18 Å was used as the lower bound. The non-covalent complex was obtained by scoring on these criteria and therefore fits with the NMR-based restraints well. In contrast, the cross-linked structure does not satisfy all the

restraints. The major violation is for the residues G70-T73 which are located far (> 20 Å) from the iron sulfur cluster in the cross-linked FTR/Trx-*m*.

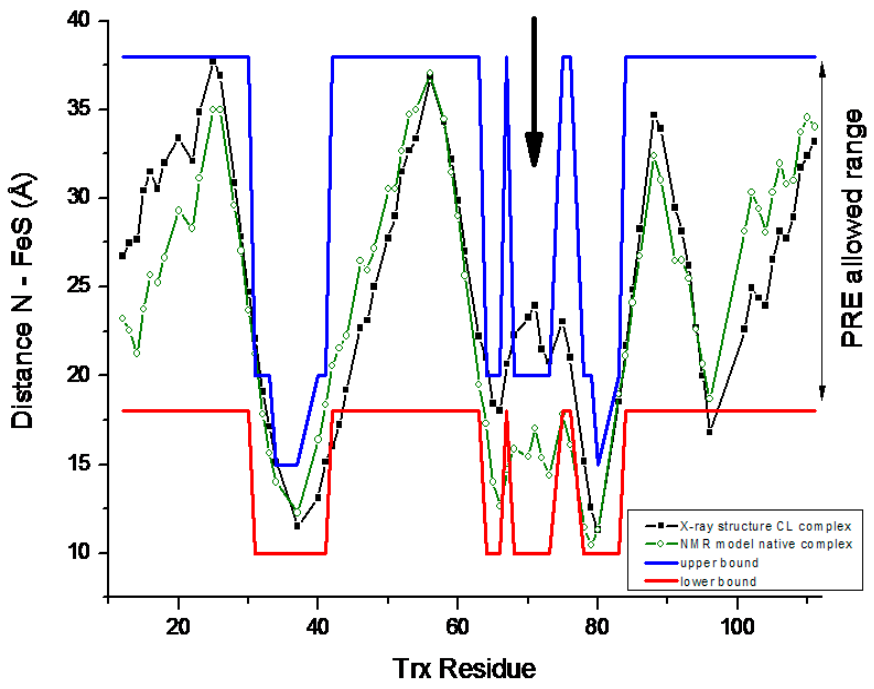

Figure 6.5. Comparison of cross-linked and non-covalent FTR/Trx-m models with paramagnetic restraints. Distances are shown between amide nitrogens of Trx-*m* and iron sulfur center in non-covalent FTR/Trx-*m* (green, circles,) and cross-linked complex (black line, squares). The blue and red lines indicate the upper bound and lower distance bounds, respectively, derived from PRE effect. Disagreement with the distance restraints of residue G70-T73 in the cross-linked FTR/Trx-*m* is marked with

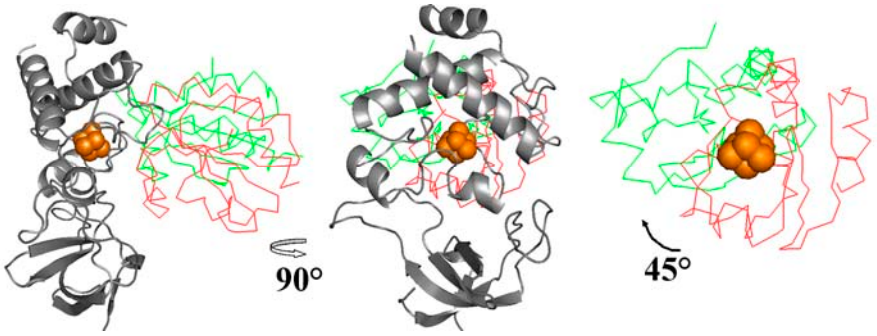

Figure 6.6. Structural comparison of non-covalent and cross-linked FTR/Trx-*m* complexes. FTR was superimposed and shown in gray ribbon. Trx-*m* conformations in non-covalent and cross-linked complexes are depicted as red and green C^{α} traces, respectively. The 4Fe-4S cluster is shown in orange spheres. In the middle panel, the structures have been rotated by 90° relative to the left panel. The right panel is like the middle panel, but FTR has been left out for clarity, except for the 4Fe-4S cluster.

These differences are borne out by a comparison of the structures (Figure 6.6). In both structures, Trx-*m* has a similar interface for docking to FTR. In the non-covalent complex, the active site cysteine C32 of Trx-*m* can get close to the C57 of FTR, whereas these two residues are disulfide-bonded in the crosslinked complex. However, the orientations of Trx-*m* relative to FTR in two structures are significantly different. In the model of non-covalent complex, the short helix G70-T73 of Trx-*m* docks partially into a concave region formed by two subunits of FTR, whereas in the crystal structure of cross-linked complex, G70-T73 of FTR has a direct contact with a loop (residue 58-61) in catalytic subunit of FTR. The comparison of these two models suggests that a rotational movement (about 45°) relative to FTR is necessary for Trx-*m* to proceed from the non-covalent to the crosslinked complex.

The dynamics coupled with thioredoxin recognition

Previous ^{15}N relaxation measurements suggested the presence of dynamics of loops and tryptophan side chain of thioredoxin *E. coli* on several time scales [(15)]. This dynamics may relate to the flexibility and plasticity of Trx interacting with other proteins for thio-disulfide exchange. Conformational fluctuation coupled with thio-disulfide transfer was found for the interaction of Trx from *B. subtilits* with arsenate reductase [(16)].

For FTR, there are several charged residues located on the side for docking to Trx. E84, D94, and D96 form an acidic patch (Figure 6.7A). FTR may use this patch as an attractant for the interaction with FTR (Figure 6.7B) which had a positive charged residue R78 close to the active site. These charged residues are highly conserved. The comparison of crystal structures of free FTR with

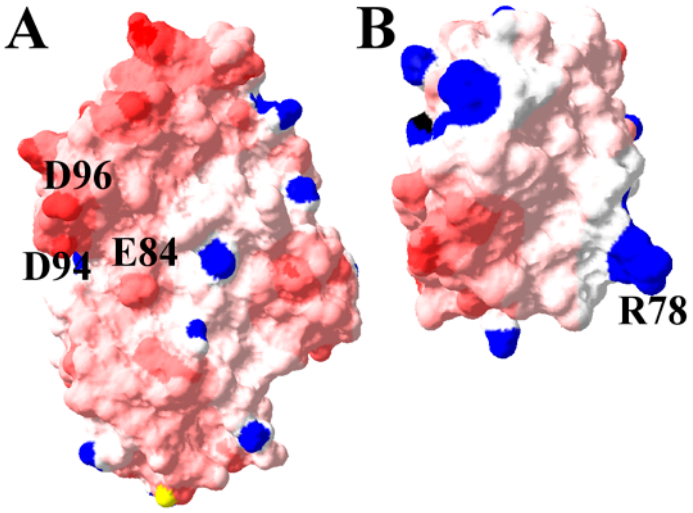

Figure 6.7. Electrostatic surface representation of the interface of FTR (A) and Trx-*m* (B) in the complex.

covalent cross-linked FTR/Trx intermediate suggests that there is no structural change for backbone conformation upon the binding. However, a local structural rearrangement of side chains for several residues of FTR is obvious. The largest

changes are for H86 and H59. In the free FTR, these two residues protruded from the surface. In contrast, in the cross-linked complex, the side chain rotation of H86 of FTR leads to a flat surface, which is correlated with the flipping of W36 of Trx-*m*. As a consequence, the flipping H59 can further remove the steric hindrance, allowing the rotational movement of Trx to sample the best surface complementarities. The result of rotation of H59 can provide the complementary surface to accommodate the short helix after the rotational movement of Trx-*m*.

The non-covalent ternary complex

The formation of ternary complex of Fd with cross-linked FTR/Trx-*m* complex has been demonstrated by gel filtration chromatography [(17)]. Our NMR titration experiments show that non-covalent binary complex formed by FTR/Trx can interact with Fd also to form a ternary complex. The elongated, flat structure of FTR seems optimal for simultaneous binding of its two substrates, enabling a flow of electrons from the 2Fe2S cluster in Fd via the 4Fe-4S cluster of FTR to the disulfide bond in Trx.

Conclusions

The interaction of Fd, FTR, and Trx-*m* in an electron-transfer chain has been studied by NMR. A non-covalent ternary complex formed in solution was demonstraged from NMR titrations. The docking model of the binary complex of Trx-*m* and FTR suggests a relative orientation change of the two proteins when the non-covalent binary complex proceeds to the covalent complex. This study shows that paramagnetic NMR and X-ray diffraction are complimentary in the study of the transient electron-transfer complex.

Reference List

1. Schurmann P. and Buchanan B.B. (2008) The ferredoxin/thioredoxin system of oxygenic photosynthesis. *Antioxidants & Redox Signaling* **10**: 1235-1273.

2. Dai S.D., Schwendtmayer C., Johansson K., Ramaswamy S., Schürmann P., and Eklund H. (2000) How does light regulate chloroplast enzymes? Structure-function studies of the ferredoxin/thioredoxin system. *Quarterly Reviews of Biophysics* **33**: 67-108.
3. Dai S.D., Johansson K., Miginiac-Maslow M., Schürmann P., and Eklund H. (2004) Structural basis of redox signaling in photosynthesis: structure and function of ferredoxin : thioredoxin reductase and target enzymes. *Photosynthesis Research* **79**: 233-248.
4. Dai S.D., Schwendtmayer C., Schürmann P., Ramaswamy S., and Eklund H. (2000) Redox signaling in chloroplasts: Cleavage of disulfides by an iron-sulfur cluster. *Science* **287**: 655-658.
5. Dai S.D., Friemann R., Glauser D.A., Bourquin F., Manieri W., Schürmann P., and Eklund H. (2007) Structural snapshots along the reaction pathway of ferredoxin-thioredoxin reductase. *Nature* **448**: 92-96.
6. Staples C.R., Ameyibor E., Fu W.G., GardetSalvi L., StrittEtter A.L., Schürmann P., Knaff D.B., and Johnson M.K. (1996) The function and properties of the iron-sulfur center in spinach ferredoxin:thioredoxin reductase: A new biological role for iron-sulfur clusters. *Biochemistry* **35**: 11425-11434.
7. Staples C.R., Gaymard E., Stritt-Etter A.L., Telser J., Hoffman B.M., Schürmann P., Knaff D.B., and Johnson M.K. (1998) Role of the Fe4S4] cluster in mediating disulfide reduction in spinach ferredoxin: Thioredoxin reductase. *Biochemistry* **37**: 4612-4620.
8. Walters E.M., Garcia-Serres R., Jarneson G.N.L., Glauser D.A., Bourquin F., Manieri W., Schürmann P., Johnson M.K., and Huynh B.H. (2005) Spectroscopic characterization of site-specific [Fe4S4] cluster chemistry in ferredoxin : thioredoxin reductase: Implications for the catalytic mechanism. *Journal of the American Chemical Society* **127**: 9612-9624.
9. Xu X.F., Kim S.K., Schürmann P., Hirasawa M., Tripathy J.N., Smith J., Knaff D.B., and Ubbink M. (2006) Ferredoxin/ferredoxin-thioredoxin reductase complex: Complete NMR mapping of the interaction site on ferredoxin by gallium substitution. *Febs Letters* **580**: 6714-6720.
10. Helgstrand M., Kraulis P., Allard P., and Härd T. (2000) Ansig for Windows: An interactive computer program for semiautomatic assignment of protein NMR spectra. *J.Biomol.NMR* **18**: 329-336.
11. Neira J.L., Gonzalez C., Toiron C., Prat-Gay G., and Rico M. (2001) Three-dimensional solution structure and stability of thioredoxin m from spinach. *Biochemistry* **40**: 15246-15256.
12. Palma P.N., Krippahl L., Wampler J.E., and Moura J.J.G. (2000) BiGGER: A new (soft) docking algorithm for predicting protein interactions. *Proteins-Structure Function and Genetics* **39**: 372-384.
13. Capitani G., Markovic-Housley Z., DelVal G., Morris M., Jansonius J.N., and Schurmann P. (2000) Crystal structures of two functionally different thioredoxins in spinach chloroplasts. *Journal of Molecular Biology* **302**: 135-154.
14. Crowley P.B. and Carrondo M.A. (2004) The architecture of the binding site in redox protein complexes: implications for fast dissociation. *Proteins* **55**: 603-612.
15. Stone M.J., Chandrasekhar K., Holmgren A., Wright P.E., and Dyson H.J. (1993) Comparison of Backbone and Tryptophan Side-Chain Dynamics of Reduced and Oxidized Escherichia-Coli Thioredoxin Using N-15 Nmr Relaxation Measurements. *Biochemistry* **32**: 426-435.
16. Li Y., Hu Y.F., Zhang X.X., Xu H.M., Lescop E., Xia B., and Jin C.W. (2007) Conformational fluctuations coupled to the thiol-disulfide transfer between thioredoxin and arsenate reductase in Bacillus subtilis. *Journal of Biological Chemistry* **282**: 11078-11083.
17. Glauser D.A., Bourquin F., Manieri W., and Schürmann P. (2004) Characterization of ferredoxin : thioredoxin reductase modified by site-directed mutagenesis. *Journal of Biological Chemistry* **279**: 16662-16669.